HHS Public Access

Author manuscript

Pharmacol Res. Author manuscript; available in PMC 2022 December 01.

Published in final edited form as:

Pharmacol Res. ; 174: 105877. doi:10.1016/j.phrs.2021.105877.

TLR4 and AT1R mediate blood-brain barrier disruption, neuroinflammation, and autonomic dysfunction in spontaneously hypertensive rats

Francesca E. Mowry, M.S., Ph.D.[1,2], **Sarah C. Peaden, B.A.**[1], **Javier E. Stern, Ph.D., M.D.**[3], **Vinicia C. Biancardi, M.S, Ph.D.**[1,2]

[1]Department of Anatomy, Physiology & Pharmacology, College of Veterinary Medicine, Auburn University, Auburn, AL, USA

[2]Center for Neurosciences Initiative, Auburn University, Auburn, AL, USA

[3]Center for Neuroinflammation, Georgia State University, Atlanta, GA, USA

Abstract

Angiotensin II (AngII) is implicated in neuroinflammation, blood-brain barrier (BBB) disruption, and autonomic dysfunction in hypertension. We have previously shown that exogenous AngII stimulates Toll-like receptor 4 (TLR4) via AngII type 1 receptor (AT1R), inducing activation of hypothalamic microglia *ex vivo*, and that AngII-AT1R signaling is necessary for the loss of BBB integrity in spontaneously hypertensive rats (SHRs). Herein, we hypothesized that microglial TLR4 and AT1R signaling interactions represent a crucial mechanistic link between AngII-mediated neuroinflammation and BBB disruption, thereby contributing to sympathoexcitation in SHRs. Male SHRs were treated with TAK-242 (TLR4 inhibitor; 2 weeks), Losartan (AT1R inhibitor; 4 weeks), or vehicle, and age-matched to control Wistar Kyoto rats (WKYs). TLR4 and AT1R inhibitions normalized increased TLR4, interleukin-6, and tumor necrosis factor-α protein densities in SHR cardioregulatory nuclei (hypothalamic paraventricular nucleus [PVN], rostral ventrolateral medulla [RVLM], and nucleus tractus solitarius [NTS]), and abolished enhanced microglial activation. PVN, RVLM, and NTS BBB permeability analyses revealed complete restoration after TAK-242 treatment, whereas SHRs presented with elevated dye leakage. Mean arterial pressure was normalized in Losartan-treated SHRs, and attenuated with TLR4 inhibition. In conscious assessments, TLR4 blockade rescued SHR baroreflex sensitivity to

Corresponding Author: Vinicia C. Biancardi, M.S., Ph.D., Anatomy, Physiology & Pharmacology, College of Veterinary Medicine, Auburn University, 217 Greene Hall, Auburn, AL – 36849, Phone: 334-844-5366/Fax: 334-844-4542, vbiancardi@auburn.edu.

Credit Author Statement

FEM: Conceptualization, Investigation, Formal analysis, Writing - Original draft preparation, Writing - Reviewing and Editing; SCP: Investigation, Writing - Reviewing and Editing; JES: Resources, Conceptualization; VCB: Resources, Conceptualization, Investigation, Formal analysis, Writing - Original draft preparation, Writing - Reviewing and Editing, Funding acquisition.

Declarations of interest: None

Chemical compounds studied in this article: TAK-242 (PubChem CID: 11703255); losartan (PubChem CID: 11751549); phenylephrine hydrochloride (PubChem CID: 5284443); sodium nitroprusside dehydrate (PubChem CID: 11953895); hexamethonium bromide (PubChem CID: 24278459)

vasoactive drugs, and reduced the SHR pressor response to ganglionic blockade to normal levels. These data suggest that TLR4 activation plays a substantial role in mediating a feed-forward pro-hypertensive cycle involving BBB disruption, neuroinflammation, and autonomic dysfunction, and that TLR4-specific therapeutic interventions may represent viable alternatives in the treatment of hypertension.

Graphical Abstract

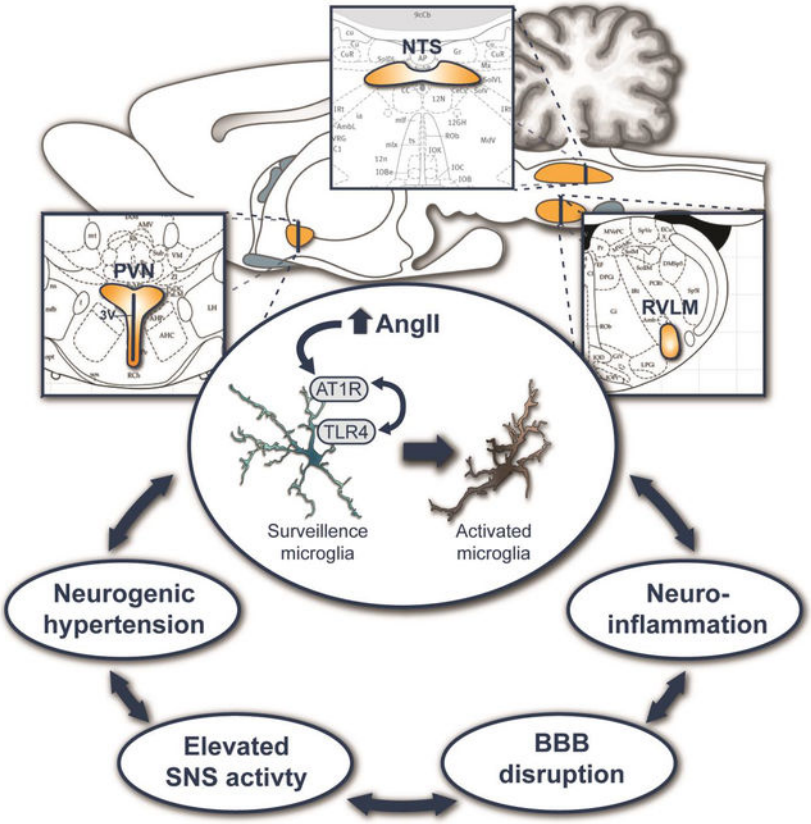

Keywords

Angiotensin II; Toll-like receptor 4; blood-brain barrier; microglia; neuroinflammation; hypertension

1. INTRODUCTION

According to the 2019 Heart Disease and Stroke Statistics, approximately 46% of Americans have hypertension[1]. Recent estimates suggest that up to 20% of patients remain resistant to currently available anti-hypertensive medications[2], highlighting the need to identify new therapeutic targets for the effective treatment of hypertension. A common observation among these patients is an elevation in sympathetic nervous system (SNS) activity[3–7]. Within the central nervous system (CNS), multiple cardioregulatory nuclei govern sympathetic outflow, including the hypothalamic paraventricular nucleus (PVN),

rostral ventrolateral medulla (RVLM), and nucleus of the tractus solitarius (NTS). In brief, whereas the PVN enhances sympathetic activity via projections to the intermediolateral spinal column and RVLM, the primary nucleus responsible for net sympathetic outflow[8, 9], the NTS suppresses RVLM activity by way of the caudal ventrolateral medulla[10]. Previous studies within these nuclei show that altered renin-angiotensin system (RAS) mechanisms, particularly dysregulation of angiotensin II (AngII) signaling, contribute to increased sympathetic activity in hypertension[11]. As AngII's type 1 receptor (AT1R) is expressed by multiple CNS cell types, AngII may influence neuronal activity directly, by binding neuronal AT1R, or indirectly, by influencing the activity of endothelial cells, perivascular macrophages[12], astrocytes[13], and microglia[14].

AngII dysregulation is strongly associated with low-grade neuroinflammation, microglial activation, and blood-brain barrier (BBB) disruption in CNS cardioregulatory nuclei[11, 15, 16]. We have shown that AngII-induced BBB breakdown facilitates entry of circulating AngII into the PVN, RVLM, and NTS of spontaneously hypertensive rats (SHRs), targeting neurons and microglia therein. Prior work consistently reports increased microglial activation and elevated levels of pro-inflammatory cytokines (PICs; i.e., tumor necrosis factor [TNF]-α, interleukin [IL]-6, and IL-1β) in the PVN of hypertensive animals in response to AngII, with several studies demonstrating clear links amid microglia, PIC signaling, and elevated sympathetic activity in SHRs[17, 18], L-N^G-nitro-l-arginine methyl ester (L-NAME)- and AngII-infusion mice[19], and AngII-infusion rats[20].

Microglia are direct regulators of the neuroinflammatory response. These innate immune cells constitutively express AT1R and Toll-like receptor 4 (TLR4)[14, 21], a pattern-recognition receptor implicated in multiple neuroinflammatory and cardiovascular diseases, including hypertension[15, 22, 23]. Upon stimulation by pathogen-associated molecular patterns (i.e., lipopolysaccharide [LPS]) or damage-associated molecular patterns[24], TLR4 initiates pro-inflammatory signaling cascades, causing microglial activation and triggering downstream PIC production. Using an *ex vivo* preparation of PVN-containing hypothalamic slices, we have demonstrated an interaction between AT1R-dependent signaling cascade(s) and TLR4 following exogenously applied AngII, such that TLR4 becomes stimulated, leading to microglial activation and reactive oxygen species (ROS) generation[14]. While various *in vivo* and *in vitro* studies have shown that AngII upregulates TLR4 expression, stimulates microglia, enhances PIC production, and disrupts the BBB[14, 15, 25, 26], the extent to which *in vivo* AT1R-TLR4 signaling interactions contribute to the etiology and preservation of a hypertensive state remains unclear.

Based on recent evidence, we hypothesized that interactions between microglial AngII-AT1R and -TLR4 signaling cascades represent a critical mechanistic link between AngII-mediated neuroinflammation and BBB disruption within the PVN, RVLM, and NTS, ultimately contributing to the maintenance of an inflammatory and sympathoexcitatory state in cases of chronic hypertension. As such, this study aimed to evaluate TLR4 as an alternative target in the treatment of hypertension by examining the efficacy of systemic TLR4 blockade in mitigating indices of neuroinflammation and autonomic dysfunction relative to the widely used AT1R inhibitor, Losartan. In addition, we explored the potential for repurposing TAK-242 (resatorvid), a specific TLR4 inhibitor originally tested in clinical

trial for the treatment of sepsis (NCT00633477) that binds Cys747 in the receptor's intracellular domain[27] and is able to cross the intact BBB[28, 29]. Using SHRs, we examined the impact of TAK-242 administration on BP changes, TLR4 protein expression, PIC production, microglial activation status, BBB integrity, baroreflex sensitivity, and indirect sympathetic activity.

2. MATERIALS AND METHODS

2.1. Animals and experimental groups

All procedures were approved by the Institutional Animal Care and Use Committee (protocol 2017–2883) and were performed in accordance with the *Guide for the Care and Use of Laboratory Animals,* as recommended by the US National Institutes of Health. Male Wistar Kyoto rats (WKY) and SHRs (Charles River Laboratories, USA) were housed in temperature- and humidity-controlled rooms (22±1°C; 50±5%) under a 12–12h light-dark cycle with standard rat chow and water *ad libitum*. Animals were 7–8 weeks old (175–225g) at the start of experiments. SHRs were randomly divided into control or experimental groups. For AT1R blockade, SHRs were treated daily with Losartan (AT1R antagonist; TCI America, USA; 20mg/kg BW[16]; oral gavage; SHR-Los) or vehicle for 4 weeks, and age-matched with WKYs (n=6/group). For TLR4 blockade, SHRs were treated daily with TAK-242 (TLR4 antagonist; Apex Bio, USA; MedChem Express, USA; 2mg/kg BW[30]; *i.p.*; SHR-TAK; n=17) for 2 weeks, and age-matched with control SHRs (n=13) and WKYs (n=11). The dose of TAK-242 was chosen based on previous work supporting suppression of cardiac and renal inflammatory cytokines levels (TNF-a, IL-1β and MCP-1) and prevention of blood pressure increases in a model of Aldosterone-induced hypertension[31].

2.2. Indirect blood pressure assessment

Indirect blood pressure (BP) measurements were performed using a volume-pressure recording tail-cuff system (CODA-6, Kent Scientific Corporation, USA)[32]. Animals were acclimated to the BP recording system for three days prior to the start of experiments. For data collection, 5 acclimation and 20 regular cycles were run, the latter of which were averaged to determine mean arterial pressure (MAP) values, as previously reported[33]. BP measurements were taken on a weekly basis for animals in the Losartan cohort. For TAK-242-treated animals and age-matched controls, BP was assessed on alternating days.

2.3. Surgical procedures

Animals were anesthetized with isoflurane (induction: 5%, maintenance: 2%) and/or a cocktail of Ketamine (100 mg/kg BW)-Xylazine (15 mg/kg BW; *i.p.*). Anesthesia levels were evaluated regularly throughout procedures by checking for absent tail- and toe-pinch reflexes.

2.3.1. Baroreceptor reflex sensitivity and indirect sympathetic activity: The abdominal aorta was cannulated through the left femoral artery to allow for continuous BP and heart rate (HR) recordings. The left femoral vein was cannulated for delivery of drugs during autonomic function assessments. Cannulae were tunneled subcutaneously and exteriorized through the mid-scapular region of the back, and lidocaine was applied

to surgical sites. Animals were given Carprofen (2.5 mg/kg BW; *s.q.*) for pain. The following day, cardiac parameters were recorded from unrestrained conscious rats by a pressure transducer (model SP 844, Memscap AS, Norway) system with computer data acquisition (Bridge Amp/PowerLab 4/35, ADInstruments, Australia). After 30 min of baseline recording, *i.v.* doses of phenylephrine (Phe; 20 μg/kg BW; MilliporeSigma, USA) and sodium nitroprusside (SNP; 25 μg/kg BW; Spectrum Chemical, USA) were randomly administered, followed by the ganglionic blocker, hexamethonium bromide (20 mg/kg BW; Sigma, USA)[34, 35]. Drug doses were separated by 10–15 min to allow cardiac parameters to return to baseline. Baroreceptor reflex sensitivity was determined by heart rate compensation for a given change in MAP (ΔHR [BPM]/ΔMAP [mmHg]), as evaluated at the maximal response. Indirect SNS activity was indexed as the magnitude of the depressor response to hexamethonium bromide, expressed as ΔMAP, relative to the 1 min period immediately prior to injection.

2.3.2. BBB permeability: BBB permeability surgeries were performed as previously described[16]. In short, a fluorescent dye cocktail of rhodamine B isothiocyanate-dextran (RHO70; 70kDa, 10 mg/mL; Sigma-Aldrich, USA) and fluorescein isothiocyanate-dextran (FITC10; 10kDa, 10 mg/mL; Sigma-Aldrich, USA) dissolved in sterile saline was injected through the left carotid artery (3 μL/g BW) and allowed to circulate for 30 min. Brains were extracted, post-fixed in 4% formaldehyde (PFA; 48 h), cryoprotected in 30% sucrose (72 h), and stored at −80°C until sectioning.

2.4. Immunohistochemistry

Brains were removed following transcardial perfusion with 150 mL 0.01M phosphate-buffered saline (PBS) and 350 mL 4% PFA. Whole brains were post-fixed in 4% PFA for 24 h, cryoprotected in a 30% sucrose solution for 72 h, and stored at −80°C prior to sectioning. Serial hypothalamic slices of 30 μm (containing the PVN) and medullary sections of 40 μm (containing the RVLM and/or NTS) were collected (Microm cryostat HM 525). Slices were stored in cryoprotectant solution (200 mL glycerol [RNAse-Free; Sigma, USA], 300 mL ethylene glycol [Aldrich, USA], 450 mL dH2O, 75 mL 0.3 M PBS) at −20°C until processing.

Slices were washed three times in PBS to remove cryoprotectant solution and incubated for 1 h with 10% normal donkey serum (Jackson ImmunoResearch, USA). Sections were incubated in PBST (0.01M PBS, 0.1% Triton, 0.04% NaN3) with 5% normal donkey serum and primary antibodies against TLR4 (mouse monoclonal IgG2bκ, 1:250, Novus Biologicals, USA, NB100–56567, lot CJU03–11 and IMG-5031A), ionized calcium-binding adaptor molecule 1 (IBA1; microglial marker [rabbit polyclonal, 1:1000, Wako Chemicals, USA, 019–19742, lot WDK2121 and WDF6884; goat polyclonal, 1:500, Abcam, UK, ab5076, lot GR3195324–1; or rabbit polyclonal, 1:2000, EnCor Biotechnology Inc., USA, RPCA-IBA1, lot 040119]), TNF-α (mouse monoclonal IgG1, 1:100, Santa Cruz Biotechnology, USA, sc-52746, lot C0119), and/or IL-6 (mouse monoclonal IgG2a, 1:100, Santa Cruz Biotechnology, USA, sc-32296, lot I2818). Hypothalamic slices were also incubated with (Arg8)-vasopressin (VP; guinea pig polyclonal, 1:5000, Peninsula Laboratories, USA, T-5048.0050, lot A17901) and brainstem sections were incubated with

tyrosine hydroxylase (TH; rabbit polyclonal [1:2000, EnCor Biotechnology Inc., USA, RPCA-TH, lot 040199] or mouse monoclonal IgG2a [1:1000, Santa Cruz Biotechnology, USA, sc-25270, lot G1917 and G1918]) for use as anatomical markers. In addition, antigen-retrieval (5 min incubation in PBS containing 1% w/v sodium dodecyl sulfate [SDS]) was performed prior to serum blocking in tissue sections used for microglial morphological analyses. Slices were washed in PBS and incubated with respective Alexa Fluor® AffiniPure Donkey IgG (H+L) secondary antibodies from Jackson ImmunoResearch: 488 anti-mouse (1:250), 594 anti-rabbit (1:250), 594 anti-guinea pig (1:250), or 647 anti-rabbit (1:50). Negative control sections were run without primary antibodies. Sections were washed and mounted with Vectashield Antifade Mounting Medium or VECTASHIELD® Antifade Mounting Medium with DAPI (Vector Laboratories, USA).

2.5. Immunofluorescence imaging and analysis

Full-thickness confocal z-stacks (1 μm intervals) of PVN-, RVLM-, and NTS-containing brain sections were acquired with a Nikon Eclipse TE2000-E inverted microscope coupled to a Nikon A1 confocal laser and analyzed using ImageJ software (NIH; https://imagej.nih.gov/ij/index.html).

2.5.1. Protein density quantification: Confocal z-stacks were taken with a 20x objective in the PVN, RVLM, and NTS (1 image/unilateral nucleus/slice, 4–6 slices/animal). TLR4, IL-6, and TNF-α immunofluorescence signals (% area), expressed as % change from WKY, were quantified from maximum projection images, as previously described[16], using ImageJ.

2.5.2. Microglia morphological analysis: Microglial activation status was examined with a skeletal analysis method adapted from Morrison and Filosa[36] using maximum projection images of IBA1 fluorescence at 60x-magnification in the PVN, RVLM, and NTS (3 images/unilateral nucleus/slice, 4–6 slices/animal). Briefly, threshold adjustments and noise reductions were applied to increase visualization of cell processes, images were converted to binary, skeletonized, and analyzed with the AnalyzeSkeleton plugin (http://github.com/fiji/AnalyzeSkeleton). The number of end points and total branch length were used as morphological parameters reflective of relative branching complexity among groups.

2.5.3. BBB permeability assessment: Dye-injected brains were cut to 40 μm-thick sections containing the PVN and 50 μm-thick sections containing the RVLM and NTS. Slices were counterstained with DAPI (VECTASHIELD® Antifade Mounting Medium with DAPI, Vector Laboratories, USA) and/or TOTO-3 Iodide (1:50,000, ThermoFisher Scientific, USA) and imaged with a 20x objective (2 images/slice [bilateral], 4–6 slices/animal). Extravasation of the low molecular weight (MW) dye ($FITC10_{EV}$) was used as an index of BBB integrity. Quantification of $FITC10_{EV}$ was achieved by subtracting colocalized FITC10 and RHO70 pixels from a maximum projection of the FITC10 channel, and measuring the percent area of $FITC10_{EV}$ from the newly generated image, as previously described[16].

2.6. Statistical Analyses

Data are reported as mean±*SEM* unless otherwise indicated. Groups were compared by one-way or two-way ANOVA with Tukey post-hoc tests. Analyses were run using GraphPad Prism 7 (GraphPad Software, Inc., USA) with statistical significance considered at $p<0.05$.

3. RESULTS

3.1. AT1R and TLR4 inhibitors decrease MAP in SHRs.

Following 4 weeks of AT1R blockade, SHR-Los MAP (103.6±2.4 mmHg), as measured via indirect tail-cuff, was normalized to similar levels as observed in WKYs (100.0±3.0 mmHg, $p=0.473$), whereas SHR MAP (154.9±1.7 mmHg, $p<0.0001$) remained significantly elevated (n=6/group; Fig. 1A). Treatment with TAK-242 attenuated the MAP increases in SHR-TAK (n=17) that were observed in SHRs (n=12) beginning on day three (142.6±3.01 vs. 161±1.5 mmHg, $p<0.0001$), and persisted throughout the rest of the treatment period (day 14: 129.5±2.8 vs. 153.8±2.1 mmHg; $p<0.0001$). SHR-TAK MAP, while reduced, was significantly greater than MAP levels in WKYs at the end of treatment (109.2±2.9 mmHg, $p<0.0001$; Fig. 1B). The trends observed in the TAK-242 cohort were confirmed in the cohort subjected to direct MAP recordings in unrestrained conscious animals at the end of treatment (WKY: 109.2±6.1 mmHg [n=5]; SHR: 169.4±13.5 mmHg [$p<0.0001$ vs. WKY, n=6]; SHR-TAK: 150.8±9.0 mmHg [$p=0.003$ vs. WKY, $p<0.0001$ vs. SHR, n=10]; Fig. 1C).

3.2. TLR4 protein expression is upregulated through AT1R and TLR4.

To examine the role of AngII-AT1R signaling in regulating TLR4 protein expression, we performed immunofluorescence assays in the PVN, RVLM, and NTS (expressed as % change from WKY, Fig. 2). Consistent with previous reports[37–39], TLR4 protein density was increased in SHR PVN compared to WKY (+133.0±14.7%, $p<0.0001$), and normalized in SHR-Los (+27.8±10.6%) and SHR-TAK (+10.7±4.9%). TLR4 expression was elevated in SHR RVLM (+107.9±6.7%, $p<0.0001$) and normalized in SHR-Los (−1.05±4.6%) and SHR-TAK (+11.3±3.1%). Similarly, NTS TLR4 expression was higher in SHR (+101.6±6.9%, $p<0.0001$), with normalization in both treatment groups (SHR-Los: +11.0±7.4%; SHR-TAK: +1.5±4.7%), suggesting a feed-forward upregulation of central TLR4 in SHRs that relies upon activation of both AT1R- and TLR4-dependent signaling pathways.

3.3. PICs are downregulated following AT1R or TLR4 blockade.

Using a semi-quantitative densitometry analysis, we examined IL-6 and TNF-α immunofluorescence in the PVN, RVLM, and NTS (expressed as % change from WKY). Protein expression of both cytokines was increased in SHR PVN (IL-6: +46.60±4.8%, $p<0.0001$; TNF-α: +57.97±8.9%, $p<0.0001$), RVLM (IL-6: +77.44±11.6%, $p<0.0001$; TNF-α: +58.01±7.9%, $p<0.0001$), and NTS (IL-6: +49.3±4.1%, $p<0.0001$; TNF-α: +56.5±4.3%, $p<0.0001$) versus WKYs. PVN cytokine expression was normalized with Losartan (IL-6: +0.85±5.0%; TNF-α: +5.99±3.9%) and TAK-242 treatment (IL-6: +1.30±2.9%; TNF-α: +5.70±2.6%; Fig. 3). NTS IL-6 and TNF-α were normalized in SHR-Los (IL-6: +8.8±6.1; TNF-α: +3.5±4.8%) and SHR-TAK (IL-6: +5.6±4.0%; TNF-α: +6.7±4.3%) (Fig. 4).

Both treatments restored RVLM TNF-α expression to baseline (SHR-Los: +8.16±4.7%; SHR-TAK: +4.48±5.2%), and reduced IL-6 (SHR-Los: +32.37±3.9% [p=0.0011 vs. WKY, p=0.0013 vs. SHR]; SHR-TAK: +33.90±7.6% [p=0.0023 vs. WKY, p=0.0017 vs. SHR]; Fig. 5), suggesting that both AT1R and TLR4 signaling mechanisms are involved in regulating the pro-inflammatory profile of CNS cardioregulatory nuclei in SHRs.

3.4. AT1R and TLR4 are necessary for microglial activation.

We quantified morphological changes of microglia using a skeletal analysis[36] of IBA1 immunostaining to index total branch number (end points) and branch length. Under normal physiological conditions, surveillance microglia present with a small soma and numerous fine, highly-ramified, motile processes. Conversely, the classically activated pro-inflammatory M1 microglial phenotype is associated with an enlarged cell soma and overall deramification, such that a relative reduction in branching complexity is reflective of increased activation towards an amoeboid phagocytotic state. Within the PVN, SHRs showed a significant reduction in end points (−36.1±3.6%, p<0.0001) and branch length (−26.8±4.7%, p<0.0001) compared to WKYs, indicating a significant increase in microglial activation in hypertensive animals relative to that observed in normotensive controls. These values were normalized in the PVN of SHR-Los (end points: 2.9±2.2%; branch length: 11.3±2.5%) and SHR-TAK (end points: 4.7±5.6%; branch length: 4.0±5.1%). The reduction in end points and branch length in SHR RVLM tissue (end points: −29.3±3.3%, p<0000.1; branch length: −26.9±2.9, p=0.0004) compared to WKY was restored in SHR-Los (end points: −4.3±1.5%; branch length: −2.9±4.8%) and SHR−TAK (end points: 3.8±4.8%; branch length: 8.7±3.7%) (Fig. 6), with a similar trend observed in the NTS (Fig. 7) of SHRs (end points: −53.1±2.0%, p<0.0001; branch length: −57.2±2.0%, p<0.0001), SHR-Los (end points: +1.7±1.7%; branch length: −7.1±1.8%), and SHR-TAK (end points: +6.8±3.2%; branch length: −3.2±3.0%). These findings confirm a regulatory role for AngII-AT1R signaling in promoting microglial activation, and support a substantial contribution of TLR4 stimulation in mediating said AngII-induced activation.

3.5. Blockade of TLR4 prevents BBB disruption.

To examine the role of TLR4 in BBB permeability alterations, we quantified the degree of extravasation of a low MW dextran-conjugated fluorescent dye ($FITC10_{EV}$) in the PVN, RVLM, and NTS of SHR-TAK (Fig. 8). As previously described[16], both FITC10 and the simultaneously injected high molecular weight dye, RHO70, are maintained within cerebral vasculature when the BBB is intact. Conversely, BBB disruption results in FITC10 leakage from the vasculature to the parenchyma, reflected by an increased $FITC10_{EV}$ % area. We found significant BBB disruption in the PVN (3.619±0.108% area, p<0.0001) and RVLM (3.62±0.11% area, p<0.0001) of control SHRs relative to WKYs (PVN: 1.56±0.05% area; RVLM: 1.57±0.06% area). Inhibition of TLR4 restored the barrier's integrity in the PVN (1.52±0.05% area) and RVLM (1.51±0.05% area). In SHR NTS, $FITC_{EV}$ was significantly greater than that observed in WKYs (3.588±0.09% area in SHR vs. 1.800±0.04% area in WKYs, p<0.0001). As in the PVN and RVLM, we found NTS $FITC10_{EV}$ to be normalized in SHR-TAK (1.801±0.0513% area). Given our prior work demonstrating a reliance of PVN, RVLM, and NTS BBB disruption upon AngII-AT1R signaling in SHRs, these data indicate that activation of TLR4 is a potential mechanism by which AngII promotes BBB disruption.

3.6. Blockade of TLR4 rescues autonomic function.

We evaluated baroreceptor-heart rate reflex (baroreflex sensitivity) in response to TAK-242 treatment using bolus *i.v.* injections of vasoactive pressor (Phe) and depressor (SNP) drugs in conscious animals during continuous direct BP and HR recording[34, 35] (Fig. 9). SHRs showed a reduced HR compensation for MAP changes compared to WKYs following Phe (−1.501±0.1 vs −2.609±0.08 ΔHR [BPM]/ΔMAP [mmHg]; $p<0.0001$) and SNP (−0.9463±0.2 vs −2.379±0.3 ΔHR/ΔMAP; $p=0.0013$). TAK-242 treatment rescued SHR responsiveness to both Phe (−2.250±0.1 ΔHR/ΔMAP; $p=0.0002$ vs SHR) and SNP (−2.181±0.2 ΔHR/ΔMAP; $p=0.0017$ vs SHR). Following baroreflex assessments, indirect sympathetic activity was evaluated as the magnitude of the depressor response to *i.v.* hexamethonium bromide[34] (Fig. 9). Compared to WKYs, SHRs exhibited a greater depressor response (−65.1±3.1 vs −46.7±4.2 ΔMAP, $p=0.0396$). Conversely, sympathetic activity was restored to normal values with TLR4 inhibition in SHR-TAK animals (−42.9±4.3 ΔMAP; $p=0.0034$ vs SHR). Together, these findings indicate that TLR4 activation is necessary for the development of baroreflex impairment and sympathoexcitation in SHRs.

4. DISCUSSION

In the present study, we investigated the relative efficacy of AT1R and TLR4 inhibitors in mitigating neuroinflammation, BBB disruption, and sympathoexcitation in hypertensive SHRs. Our results demonstrate that TLR4 inhibition combats TLR4 and PIC upregulation, abolishes microglial activation, and preserves BBB integrity in the PVN, RVLM, and NTS of SHRs. Likewise, AT1R blockade normalizes TLR4 expression and microglial activation in the PVN, RVLM, and NTS of SHRs, and reduces PIC expression in these nuclei to the same extent as TLR4 inhibition. Furthermore, TLR4 blockade attenuates the progression of MAP increases in SHRs and protects against autonomic dysfunction. These findings support a significant role for TLR4 activation in the maintenance of central pro-hypertensive pathophysiology and suggest that TLR4 represents a viable alternative target in the treatment of resistant hypertension.

A number of studies implicate TLR4 activity throughout the body in the pathophysiology of hypertension (see[23, 40]). With regards to the CNS, the majority of studies have focused on alterations either within the PVN or following targeted PVN interventions. For instance, upregulation of PVN TLR4 mRNA and protein expression has been reported in multiple models of hypertension[37–39, 41–43]. Specific blockade of PVN TLR4 with TAK-242 reduces local PICs, mitigates sympathetic activity, and lowers BP in salt-induced[37, 41] and Goldblatt two kidney, one clip models of hypertension[43]. PVN-specific AT1R inhibition similarly decreases TLR4-dependent TNF-α, IL-1β, and IL-6 levels in SHRs[38]. Ogawa *et al.* have demonstrated that brainstem TLR4 stimulation via AT1R contributes to elevated sympathetic activity in chronic heart failure[44], and that silencing brain TLR4 RNA dampens sympathetic activity and ameliorates the cardiac remodeling observed in this disease pathology[45]. However, to the best of our knowledge, the relative contribution of TLR4 activation to alterations within cardioregulatory nuclei of the brainstem has yet to be investigated in a genetic model of hypertension. Importantly, minimally invasive long-term systemic TLR4

blockade has yet to be investigated as a potential intervention strategy for patients presenting with resistant hypertension.

Consistent with the aforementioned studies, we found increases in TLR4, TNF-α, and IL-6 protein expressions in the PVN of SHRs that were dependent upon AT1R and TLR4 activation. Within the RVLM and NTS, we observed that TLR4 was likewise increased in an AT1R- and TLR4-dependent manner in SHRs, pointing to a feed-forward mechanism of TLR4 upregulation in each of the cardioregulatory nuclei examined. Despite the consistency of the trends observed across both excitatory and inhibitory cardioregulatory nuclei in treated versus untreated animals, it is likely that the specific mechanisms involved in creating and maintaining the pro-inflammatory milieu varies between nuclei. Whereas heightened TNF-α levels in the RVLM were normalized following AT1R or TLR4 blockade, IL-6 expression, while reduced relative to untreated SHRs, remained elevated compared to normotensive animals. Interestingly, while SHR TNF-α increased to a similar extent within all three nuclei, the magnitude of increased IL-6 expression was approximately 30% greater in the RVLM than in the PVN or NTS. The observation that AT1R and TLR4 blockades reduce RVLM IL-6 levels to +32.37% and +33.90% relative to WKYs, respectively, points to separate AT1R- and TLR4-independent mechanism(s) of IL-6 upregulation in the RVLM of SHRs that is absent in the PVN and NTS. Of note, we recently reported on PICs within CNS cardioregulatory nuclei of SHRs treated with a probiotic (kefir) and observed a similar trend – PVN IL-6 expression was normalized in SHRs following treatment, whereas RVLM IL-6 expression remained elevated relative to WKYs by a magnitude corresponding to the difference between RVLM and PVN IL-6 levels in the untreated SHRs[33]. Based on the evidenced RAS-[46] and TLR4-[47] modulatory capabilities of kefir, it is possible that a similar mechanism is responsible for the persistence of elevated RVLM IL-6 expression in kefir-, Losartan-, and TAK-242-treated SHRs.

Within the CNS, TLR4 is primarily expressed by microglia, with relatively low levels detected in astrocytes and neurons[21, 48]. The presence of AT1R in microglia allows for AngII-mediated microglial activation[14], leading to increased ROS production and PIC synthesis. Moreover, the neuroinflammatory effects of AngII via microglial AT1R are evidenced factors underlying sympathoexcitation in neurogenic hypertension[15, 20, 49]. Microglial inhibition in the PVN blunts the hypertensive response to AngII[20]. Upon targeted microglial deletion in AngII- and L-NAME-induced hypertension, Shen *et al.* observed a significant drop in blood pressure, neuroinflammation, renal norepinephrine, and circulating arginine vasopressin[19]. We have previously demonstrated that the ability of AngII to increase PVN microglial density and ROS production is dependent upon the presence of functional TLR4[14]. Herein, we found microglial activation in SHRs to be normalized in the PVN, RVLM, and NTS following either AT1R or TLR4 inhibition. The reductions in end points and branch lengths observed in SHRs suggest that the majority of microglia in these nuclei are chronically activated, likely towards an M1/pro-inflammatory phenotype. The M1 state is well evidenced to be induced by pro-inflammatory factors and pathogens, with TLR4 stimulation considered one of the primary activation pathways. In addition to the cytotoxic and pro-inflammatory activity of these cells, M1 microglia are known to be associated with altered BBB permeability[50]. Thus, despite the inability to differentiate between classically activated M1 microglia and alternatively activated M2 microglia based

on morphology alone, it is reasonable to suspect that the deramification seen in SHR nuclei results from M1/pro-inflammatory microglial polarization. A recent study by Cohen *et al.* (2019) employed a similar skeletal analysis technique to examine microglia in the RVLM of 15-week-old SHRs, reporting decreased microglial density and branch length, with no differences in branch number or end points compared to WKYs[51]. One potential explanation for our observation of end point reductions is the difference in age, our studies being carried out at approximately 12 weeks of age. However, we would suggest that these differences are likely due to variations in staining and imaging techniques that allowed for enhanced visualization of fine microglial processes.

The potential contribution of astrocytic and/or neuronal TLR4 to the pro-hypertensive CNS milieu in SHRs cannot be disregarded. However, the evidenced effects of TLR4 activation in non-microglial cells of the CNS may indicate that microglial TLR4 stimulation is a primary mechanism. Interestingly, Liddelow *et al.* (2017) demonstrated that *in vivo* A1 activation of astrocytes (i.e., neurotoxic/pro-inflammatory activation) is absent in mice lacking microglia ($Csf1r^{-/-}$ knock-out)[52]. Indeed, mixed reports appear regarding the expression of astrocytic TLR4 and its downstream signaling components in rodents. Whether these observations are due to differences in species and/or strain, astrocyte activation state, or regional differences in astrocyte gene profiles is unknown. However, the ability of microglia to induce A1 astrocyte activation through TNF-α, IL-1α, and complement component 1q secretion[52] following LPS stimulation supports the notion of astrocyte reactivity as a secondary event in neuroinflammation.

The recognition of BBB disruption as a pathological phenomenon is increasing across an array of neurological disorders associated with neuroinflammation, including Alzheimer's disease, Parkinson's disease, and multiple sclerosis. BBB breakdown is apparent in hypertensive models[53, 54], and our prior work with Losartan-treated SHRs demonstrated such disruption to be dependent upon AngII via AT1R[16]. A subsequent study by Buttler *et al.* (2017) found disruption within autonomic centers in SHRs to increase between 1 and 3 months of age – dye leakage was absent in pre-hypertensive 4-week-old animals and, in agreement with our work, apparent at 12 weeks[55]. Herein we report marked disruption at 9–10 weeks of age in the PVN, RVLM, and NTS of SHRs, during the establishing phase of hypertension. That SHR-TAK exhibited full barrier integrity raises the question of protection versus restoration. Moreover, whether the normalization of BBB permeability following TLR4 inhibition was due to protection against initial disruptions or a result of BBB repair processes is unknown. Given the indications of a time-course association between dye leakage and BP elevation, we suggest the latter explanation, wherein the already developing hypertension points to a loss of BBB integrity by 7–8 weeks in SHRs. While either scenario illustrates a clear role for TLR4 activation in BBB disruption, the distinction between them is particularly important from a clinical standpoint due to the evidenced disruption in cases of chronic hypertension, as well as in other neuroinflammatory diseases. To that end, further investigation regarding the timeline of BBB disruption in hypertension and the potential for BBB restoration via TLR4 inhibition is undoubtedly warranted.

Although hypertension is not fully established in SHRs at 7–8 weeks, a number of studies show that key characteristics of resistant hypertension (i.e., increased sympathetic

neurotransmission) manifest prior to elevations in blood pressure, thus contributing to disease pathogenesis, as opposed to developing subsequent to the establishment of hypertension. For example, in pre-hypertensive SHRs (4 weeks of age), while arterial blood pressure is not different from age- and weight-matched WKY controls, plasma levels of the sympathetic co-transmitter NPY is increased and dysregulation in cardiac adrenergic signaling is already apparent[56]. Within the CNS, SHRs as young as 9–16 days post-natal present with increased sympathetic nervous activity, as reflected by amplified respiratory-sympathetic coupling[57]. In humans, increased sympathetic activity has been shown in borderline hypertensive patients, and enhanced pressor responses in normotensive individuals have been shown to predict the development of hypertension later in life[58]. Thus, it is likely that, rather than preventing the development of TLR4- and AT1R-dependent hypertensive pathologies outright, the pharmacological interventions employed were sufficient to normalize/attenuate the majority of parameters investigated. Taken in combination with the aforementioned studies, this would indicate that the characteristics of resistant hypertensive pathophysiology are already apparent by 7–8 weeks in SHRs. However, it is possible that the alterations in sympathetic regulation observed prior to blood pressure elevations similarly precede the development of neuroinflammation and blood-brain barrier disruption. In this regard, the question of prophylactic vs. therapeutic warrants further investigation, as does the question of relative treatment efficacy at various time points over the course of disease progression.

Consistent with previous findings, we confirmed that 2 weeks of systemic TAK-242 reduced MAP in SHRs. Bomfim *et al.* observed reductions in MAP (approx. 20mmHg) in 15-week-old SHRs treated with an anti-TLR4 antibody (1μg/day, *i.p.*) for 15 days[59]. Dange *et al.* reported a similar reduction following targeted bilateral PVN administration of VIPER (viral inhibitory peptide of TLR4; 40 μg/kg/day) for 14 days in 10–12-week-old SHRs[37]. Despite the continued elevation of MAP in SHR-TAK versus WKY, the physiological relevance of the attenuated pressure should be considered. Moreover, while still presenting with elevated BP, the overwhelming majority of the other parameters examined in this study were normalized, which may suggest some threshold BP whose associated pathological changes are responsible for inciting neuroinflammation, BBB disruption, and autonomic dysfunction. Conversely, taking into account our prior work showing that a reduction of BP alone is insufficient to remedy these pathological alterations, it may be that their normalization occurs prior to BP reductions. As discussed above, a time-course evaluation of the pathological changes examined herein relative to the development of hypertension is necessary to address this point. Additionally, the question of long-term treatment with TAK-242 has yet to be investigated, and it would be of great interest to determine whether further MAP reductions occur beyond 2 weeks.

RAS-driven aberrations in baroreflex and autonomic function are well documented in hypertension. AngII increases neuronal activity within CNS cardiovascular nuclei, a process demonstrated to contribute to the maintenance of neurogenic hypertension[15, 20, 49, 60]. Prior studies show that intracerebroventricular (*i.c.v.*) injection of LPS induces sympathetic hyperactivity through upregulation of PIC[61], whereas PVN VIPER microinjection drastically reduces plasma norepinephrine in SHRs[37]. In agreement with these studies,

our results indicate that autonomic dysfunction was abolished in SHR-TAK, as indexed by baroreflex sensitivity and indirect SNS activity.

Whereas systemic TLR4 blockade precludes us from identifying a specific effector location responsible for the findings herein, the administration route and pharmacological agent employed in this study are clinically significant. TAK-242 has already received FDA approval, and the efficacy of less invasive treatment (i.e., *i.p.* versus *i.c.v.*) to facilitate improvements in the investigated parameters provide a clear basis for further studies regarding repurposing of TAK-242. Additionally, it should be considered that the ability of TAK-242 to cross the BBB, whether intact or disrupted, would result in non-specific inhibition if directly administered *i.c.v.*. Moreover, regardless of the primary site of action, the physiological impact of TAK-242 administration on autonomic function and within cardioregulatory nuclei is evident. It is imperative to note the studies reported herein were conducted using male SHRs. Previous work targeting pro-inflammatory and/or pro-oxidative pathways have revealed sexually dimorphic responses in both animal models and clinical trials[62]. As such, the efficacy of TAK-242 in combating those central hypertensive pathophysiological processes investigated in this work are, as yet, limited to males. Additional studies are necessary to determine the extent of TLR4's contribution to the female hypertensive state.

4.1. Conclusions

In summary, the present work demonstrates a clear contribution of chronic TLR4 and AT1R activation in SHRs to 1) neuroinflammation via TLR4 upregulation, microglial activation, and pro-inflammatory cytokine production within the PVN, RVLM, and NTS; 2) BBB disruption in the PVN, RVLM, and NTS; 3) baroreflex desensitization; 4) sympathoexcitation; and 5) the progression of hypertension development. The alleviation of neuroinflammatory and sympathoexcitatory indices as investigated herein subsequent to long-term treatment with the TLR4 antagonist, TAK-242, support the further evaluation of this therapeutic as an alternative option in the treatment of resistant hypertension. Furthermore, the reliance of TLR4 protein upregulation upon AT1R activation, in combination with the consistent effects of AT1R and TLR4 inhibition on those parameters investigated, provides support for TLR4 activation as a mechanism of AngII-AT1R-dependent neuroinflammation and BBB disruption in multiple cardioregulatory nuclei, as well as autonomic dysfunction in hypertensive pathophysiology.

Acknowledgements:

The authors would like to thank Dr. Mirian Silva for her assistance and expertise with animal care and blood pressure monitoring during the treatment phase of this work.

Funding:

This work was supported by American Heart Association Scientific Development Grant, United States, 14SDG204000015 (to V. C. Biancardi), and National Institute of Neurological Disorders and Stroke Grant, United States, NS094640 (to J. E. Stern).

ABBREVIATIONS

AngII	Angiotensin II
AT1R	Angiotensin II type 1 receptor
BBB	blood-brain barrier
BP	blood pressure
BPM	beats per minute
CNS	central nervous system
FITC10	fluorescein isothiocyanate-dextran
HR	heart rate
i.c.v.	intracerebroventricular
IBA1	ionized calcium-binding adaptor molecule 1
IL	interleukin
L-NAME	L-N^G-nitro-l-arginine methyl ester
LPS	lipopolysaccharide
MAP	mean arterial pressure
MW	molecular weight
NTS	nucleus tractus solitarius
PBS	phosphate buffered saline
PFA	paraformaldehyde
Phe	phenylephrine
PIC	pro-inflammatory cytokine
PVN	hypothalamic paraventricular nucleus
RAS	renin-angiotenisin system
RHO70	rhodamine B isothiocyanate-dextran
ROS	reactive oxygen species
RVLM	rostral ventrolateral medulla
SHR	spontaneously hypertensive rat
SNP	sodium nitroprusside
SNS	sympathetic nervous system

TH	tyrosine hydroxylase
TLR4	Toll-like receptor 4
TNF	tumor necrosis factor
VIPER	viral inhibitory peptide of TLR4
VP	vasopressin
WKY	Wistar Kyoto rat

REFERENCES

1. Benjamin EJ, Muntner P, Alonso A, Bittencourt MS, Callaway CW, Carson AP, Chamberlain AM, Chang AR, Cheng S, Das SR, Delling FN, Djousse L, Elkind MSV, Ferguson JF, Fornage M, Jordan LC, Khan SS, Kissela BM, Knutson KL, Kwan TW, Lackland DT, Lewis TT, Lichtman JH, Longenecker CT, Loop MS, Lutsey PL, Martin SS, Matsushita K, Moran AE, Mussolino ME, O'Flaherty M, Pandey A, Perak AM, Rosamond WD, Roth GA, Sampson UKA, Satou GM, Schroeder EB, Shah SH, Spartano NL, Stokes A, Tirschwell DL, Tsao CW, Turakhia MP, VanWagner LB, Wilkins JT, Wong SS, Virani SS, American Heart Association Council on E, Prevention Statistics C, Stroke Statistics S. Heart disease and stroke statistics-2019 update: A report from the american heart association. Circulation. 2019;139:e56–e528 [PubMed: 30700139]
2. Carey RM, Sakhuja S, Calhoun DA, Whelton PK, Muntner P. Prevalence of apparent treatment-resistant hypertension in the united states. Hypertension. 2019;73:424–431 [PubMed: 30580690]
3. DiBona GF. Sympathetic nervous system and hypertension. Hypertension. 2013;61:556–560 [PubMed: 23357181]
4. Grassi G, Mark A, Esler M. The sympathetic nervous system alterations in human hypertension. Circ Res. 2015;116:976–990 [PubMed: 25767284]
5. Guyenet PG, Stornetta RL, Souza G, Abbott SBG, Brooks VL. Neuronal networks in hypertension: Recent advances. Hypertension. 2020;76:300–311 [PubMed: 32594802]
6. Mann SJ. Neurogenic hypertension: Pathophysiology, diagnosis and management. Clin Auton Res. 2018;28:363–374 [PubMed: 29974290]
7. Stocker SD, Kinsman BJ, Sved AF. Recent advances in neurogenic hypertension: Dietary salt, obesity, and inflammation. Hypertension. 2017
8. Guyenet PG, Stornetta RL, Holloway BB, Souza G, Abbott SBG. Rostral ventrolateral medulla and hypertension. Hypertension. 2018;72:559–566 [PubMed: 30354763]
9. Dampney RA, Michelini LC, Li DP, Pan HL. Regulation of sympathetic vasomotor activity by the hypothalamic paraventricular nucleus in normotensive and hypertensive states. Am J Physiol Heart Circ Physiol. 2018;315:H1200–H1214 [PubMed: 30095973]
10. Zoccal DB, Furuya WI, Bassi M, Colombari DS, Colombari E. The nucleus of the solitary tract and the coordination of respiratory and sympathetic activities. Front Physiol. 2014;5:238 [PubMed: 25009507]
11. Young CN, Davisson RL. Angiotensin-ii, the brain, and hypertension: An update. Hypertension. 2015;66:920–926 [PubMed: 26324508]
12. Santisteban MM, Ahn SJ, Lane D, Faraco G, Garcia-Bonilla L, Racchumi G, Poon C, Schaeffer S, Segarra SG, Korbelin J, Anrather J, Iadecola C. Endothelium-macrophage crosstalk mediates blood-brain barrier dysfunction in hypertension. Hypertension. 2020;76:795–807 [PubMed: 32654560]
13. Stern JE, Son S, Biancardi VC, Zheng H, Sharma N, Patel KP. Astrocytes contribute to angiotensin ii stimulation of hypothalamic neuronal activity and sympathetic outflow. Hypertension. 2016;68:1483–1493 [PubMed: 27698069]
14. Biancardi VC, Stranahan AM, Krause EG, de Kloet AD, Stern JE. Cross talk between at1 receptors and toll-like receptor 4 in microglia contributes to angiotensin ii-derived ros production in the

hypothalamic paraventricular nucleus. Am J Physiol Heart Circ Physiol. 2016;310:H404–415 [PubMed: 26637556]

15. Zubcevic J, Waki H, Raizada MK, Paton JF. Autonomic-immune-vascular interaction: An emerging concept for neurogenic hypertension. Hypertension. 2011;57:1026–1033 [PubMed: 21536990]
16. Biancardi VC, Son SJ, Ahmadi S, Filosa JA, Stern JE. Circulating angiotensin ii gains access to the hypothalamus and brain stem during hypertension via breakdown of the blood-brain barrier. Hypertension. 2014;63:572–579 [PubMed: 24343120]
17. Shi Z, Gan XB, Fan ZD, Zhang F, Zhou YB, Gao XY, De W, Zhu GQ. Inflammatory cytokines in paraventricular nucleus modulate sympathetic activity and cardiac sympathetic afferent reflex in rats. Acta Physiol (Oxf). 2011;203:289–297 [PubMed: 21624097]
18. Song XA, Jia LL, Cui W, Zhang M, Chen W, Yuan ZY, Guo J, Li HH, Zhu GQ, Liu H, Kang YM. Inhibition of tnf-alpha in hypothalamic paraventricular nucleus attenuates hypertension and cardiac hypertrophy by inhibiting neurohormonal excitation in spontaneously hypertensive rats. Toxicol Appl Pharmacol. 2014;281:101–108 [PubMed: 25223692]
19. Shen XZ, Li Y, Li L, Shah KH, Bernstein KE, Lyden P, Shi P. Microglia participate in neurogenic regulation of hypertension. Hypertension. 2015;66:309–316 [PubMed: 26056339]
20. Shi P, Diez-Freire C, Jun JY, Qi Y, Katovich MJ, Li Q, Sriramula S, Francis J, Sumners C, Raizada MK. Brain microglial cytokines in neurogenic hypertension. Hypertension. 2010;56:297–303 [PubMed: 20547972]
21. Olson JK, Miller SD. Microglia initiate central nervous system innate and adaptive immune responses through multiple tlrs. J Immunol. 2004;173:3916–3924 [PubMed: 15356140]
22. Biancardi VC, Bomfim GF, Reis WL, Al-Gassimi S, Nunes KP. The interplay between angiotensin ii, tlr4 and hypertension. Pharmacol Res. 2017;120:88–96 [PubMed: 28330785]
23. Nunes KP, de Oliveira AA, Mowry FE, Biancardi VC. Targeting toll-like receptor 4 signalling pathways: Can therapeutics pay the toll for hypertension? Br J Pharmacol. 2019;176:1864–1879 [PubMed: 29981161]
24. Kawai T, Akira S. Toll-like receptors and their crosstalk with other innate receptors in infection and immunity. Immunity. 2011;34:637–650 [PubMed: 21616434]
25. Benicky J, Sanchez-Lemus E, Honda M, Pang T, Orecna M, Wang J, Leng Y, Chuang DM, Saavedra JM. Angiotensin ii at1 receptor blockade ameliorates brain inflammation. Neuropsychopharmacology. 2011;36:857–870 [PubMed: 21150913]
26. Benicky J, Sanchez-Lemus E, Pavel J, Saavedra JM. Anti-inflammatory effects of angiotensin receptor blockers in the brain and the periphery. Cell Mol Neurobiol. 2009;29:781–792 [PubMed: 19259805]
27. Takashima K, Matsunaga N, Yoshimatsu M, Hazeki K, Kaisho T, Uekata M, Hazeki O, Akira S, Iizawa Y, Ii M. Analysis of binding site for the novel small-molecule tlr4 signal transduction inhibitor tak-242 and its therapeutic effect on mouse sepsis model. Br J Pharmacol. 2009;157:1250–1262 [PubMed: 19563534]
28. Hua F, Tang H, Wang J, Prunty MC, Hua X, Sayeed I, Stein DG. Tak-242, an antagonist for toll-like receptor 4, protects against acute cerebral ischemia/reperfusion injury in mice. J Cereb Blood Flow Metab. 2015;35:536–542 [PubMed: 25586141]
29. Wang YC, Wang PF, Fang H, Chen J, Xiong XY, Yang QW. Toll-like receptor 4 antagonist attenuates intracerebral hemorrhage-induced brain injury. Stroke. 2013;44:2545–2552 [PubMed: 23839500]
30. Rice TW, Wheeler AP, Bernard GR, Vincent JL, Angus DC, Aikawa N, Demeyer I, Sainati S, Amlot N, Cao C, Ii M, Matsuda H, Mouri K, Cohen J. A randomized, double-blind, placebo-controlled trial of tak-242 for the treatment of severe sepsis. Crit Care Med. 2010;38:1685–1694 [PubMed: 20562702]
31. Zhang Y, Peng W, Ao X, Dai H, Yuan L, Huang X, Zhou Q. Tak-242, a toll-like receptor 4 antagonist, protects against aldosterone-induced cardiac and renal injury. PLoS One. 2015;10:e0142456 [PubMed: 26556241]

32. Feng M, Whitesall S, Zhang Y, Beibel M, D'Alecy L, DiPetrillo K. Validation of volume-pressure recording tail-cuff blood pressure measurements. Am J Hypertens. 2008;21:1288–1291 [PubMed: 18846043]
33. de Almeida Silva M, Mowry FE, Peaden SC, Andrade TU, Biancardi VC. Kefir ameliorates hypertension via gut-brain mechanisms in spontaneously hypertensive rats. J Nutr Biochem. 2020;77:108318 [PubMed: 31923755]
34. Ameer OZ, Hildreth CM, Phillips JK. Sympathetic overactivity prevails over the vascular amplifier phenomena in a chronic kidney disease rat model of hypertension. Physiol Rep. 2014;2
35. Cavalcanti CO, Alves RR, de Oliveira AL, Cruz JC, de Franca-Silva MS, Braga VA, Balarini CM. Inhibition of pde5 restores depressed baroreflex sensitivity in renovascular hypertensive rats. Front Physiol. 2016;7:15 [PubMed: 26858657]
36. Morrison HW, Filosa JA. A quantitative spatiotemporal analysis of microglia morphology during ischemic stroke and reperfusion. J Neuroinflammation. 2013;10:4 [PubMed: 23311642]
37. Dange RB, Agarwal D, Teruyama R, Francis J. Toll-like receptor 4 inhibition within the paraventricular nucleus attenuates blood pressure and inflammatory response in a genetic model of hypertension. J Neuroinflammation. 2015;12:31 [PubMed: 25879545]
38. Li HB, Li X, Huo CJ, Su Q, Guo J, Yuan ZY, Zhu GQ, Shi XL, Liu JJ, Kang YM. Tlr4/myd88/nf-kappab signaling and ppar-gamma within the paraventricular nucleus are involved in the effects of telmisartan in hypertension. Toxicol Appl Pharmacol. 2016;305:93–102 [PubMed: 27292124]
39. Xu ML, Yu XJ, Zhao JQ, Du Y, Xia WJ, Su Q, Du MM, Yang Q, Qi J, Li Y, Zhou SW, Zhu GQ, Li HB, Kang YM. Calcitriol ameliorated autonomic dysfunction and hypertension by down-regulating inflammation and oxidative stress in the paraventricular nucleus of shr. Toxicol Appl Pharmacol. 2020;394:114950 [PubMed: 32147540]
40. Nunes KP, de Oliveira AA, Lima VV, Webb RC. Toll-like receptor 4 and blood pressure: Lessons from animal studies. Front Physiol. 2019;10:655 [PubMed: 31191352]
41. Dange RB, Agarwal D, Masson GS, Vila J, Wilson B, Nair A, Francis J. Central blockade of tlr4 improves cardiac function and attenuates myocardial inflammation in angiotensin ii-induced hypertension. Cardiovasc Res. 2014;103:17–27 [PubMed: 24667851]
42. Yang Q, Yu XJ, Su Q, Yi QY, Song XA, Shi XL, Li HB, Qi J, Zhu GQ, Kang YM. Blockade of c-src within the paraventricular nucleus attenuates inflammatory cytokines and oxidative stress in the mechanism of the tlr4 signal pathway in salt-induced hypertension. Neurosci Bull. 2020;36:385–395 [PubMed: 31641986]
43. Qi J, Yu XJ, Fu LY, Liu KL, Gao TT, Tu JW, Kang KB, Shi XL, Li HB, Li Y, Kang YM. Exercise training attenuates hypertension through tlr4/myd88/nf-kappab signaling in the hypothalamic paraventricular nucleus. Front Neurosci. 2019;13:1138 [PubMed: 31708733]
44. Ogawa K, Hirooka Y, Kishi T, Sunagawa K. Brain at1 receptor activates the sympathetic nervous system through toll-like receptor 4 in mice with heart failure. J Cardiovasc Pharmacol. 2011;58:543–549 [PubMed: 21822148]
45. Ogawa K, Hirooka Y, Kishi T, Ide T, Sunagawa K. Partially silencing brain toll-like receptor 4 prevents in part left ventricular remodeling with sympathoinhibition in rats with myocardial infarction-induced heart failure. PLoS One. 2013;8:e69053 [PubMed: 23874864]
46. Brasil GA, Silva-Cutini MA, Moraes FSA, Pereira TMC, Vasquez EC, Lenz D, Bissoli NS, Endringer DC, de Lima EM, Biancardi VC, Maia JF, de Andrade TU. The benefits of soluble non-bacterial fraction of kefir on blood pressure and cardiac hypertrophy in hypertensive rats are mediated by an increase in baroreflex sensitivity and decrease in angiotensin-converting enzyme activity. Nutrition. 2018;51–52:66–72
47. Gomez-Guzman M, Toral M, Romero M, Jimenez R, Galindo P, Sanchez M, Zarzuelo MJ, Olivares M, Galvez J, Duarte J. Antihypertensive effects of probiotics lactobacillus strains in spontaneously hypertensive rats. Mol Nutr Food Res. 2015;59:2326–2336 [PubMed: 26255877]
48. Gorina R, Font-Nieves M, Marquez-Kisinousky L, Santalucia T, Planas AM. Astrocyte tlr4 activation induces a proinflammatory environment through the interplay between myd88-dependent nfkappab signaling, mapk, and jak1/stat1 pathways. Glia. 2011;59:242–255 [PubMed: 21125645]

49. Waki H, Gouraud SS, Maeda M, Raizada MK, Paton JF. Contributions of vascular inflammation in the brainstem for neurogenic hypertension. Respir Physiol Neurobiol. 2011;178:422–428 [PubMed: 21601658]
50. Ronaldson PT, Davis TP. Regulation of blood-brain barrier integrity by microglia in health and disease: A therapeutic opportunity. J Cereb Blood Flow Metab. 2020;40:S6–S24 [PubMed: 32928017]
51. Cohen EM, Mohammed S, Kavurma M, Nedoboy PE, Cartland S, Farnham MMJ, Pilowsky PM. Microglia in the rvlm of shr have reduced p2y12r and cx3cr1 expression, shorter processes, and lower cell density. Auton Neurosci. 2019;216:9–16 [PubMed: 30598122]
52. Liddelow SA, Guttenplan KA, Clarke LE, Bennett FC, Bohlen CJ, Schirmer L, Bennett ML, Munch AE, Chung WS, Peterson TC, Wilton DK, Frouin A, Napier BA, Panicker N, Kumar M, Buckwalter MS, Rowitch DH, Dawson VL, Dawson TM, Stevens B, Barres BA. Neurotoxic reactive astrocytes are induced by activated microglia. Nature. 2017;541:481–487 [PubMed: 28099414]
53. Fernandes MV, Rosso Melo M, Mowry FE, Lucera GM, Lauar MR, Frigieri G, Biancardi VC, Menani JV, Colombari DSA, Colombari E. Intracranial pressure during the development of renovascular hypertension. Hypertension. 2021;77:1311–1322 [PubMed: 33689460]
54. Yao ST, May CN. Intra-carotid angiotensin ii activates tyrosine hydroxylase-expressing rostral ventrolateral medulla neurons following blood-brain barrier disruption in rats. Neuroscience. 2013;245:148–156 [PubMed: 23608099]
55. Buttler L, Jordao MT, Fragas MG, Ruggeri A, Ceroni A, Michelini LC. Maintenance of blood-brain barrier integrity in hypertension: A novel benefit of exercise training for autonomic control. Front Physiol. 2017;8:1048 [PubMed: 29311978]
56. Shanks J, Manou-Stathopoulou S, Lu CJ, Li D, Paterson DJ, Herring N. Cardiac sympathetic dysfunction in the prehypertensive spontaneously hypertensive rat. Am J Physiol Heart Circ Physiol. 2013;305:H980–986 [PubMed: 23913706]
57. Simms AE, Paton JF, Pickering AE, Allen AM. Amplified respiratory-sympathetic coupling in the spontaneously hypertensive rat: Does it contribute to hypertension? J Physiol. 2009;587:597–610 [PubMed: 19064613]
58. Mancia G, Grassi G. The autonomic nervous system and hypertension. Circ Res. 2014;114:1804–1814 [PubMed: 24855203]
59. Bomfim GF, Dos Santos RA, Oliveira MA, Giachini FR, Akamine EH, Tostes RC, Fortes ZB, Webb RC, Carvalho MH. Toll-like receptor 4 contributes to blood pressure regulation and vascular contraction in spontaneously hypertensive rats. Clin Sci (Lond). 2012;122:535–543 [PubMed: 22233532]
60. Kang YM, Ma Y, Zheng JP, Elks C, Sriramula S, Yang ZM, Francis J. Brain nuclear factor-kappa b activation contributes to neurohumoral excitation in angiotensin ii-induced hypertension. Cardiovasc Res. 2009;82:503–512 [PubMed: 19246475]
61. Zhang ZH, Yu Y, Wei SG, Felder RB. Centrally administered lipopolysaccharide elicits sympathetic excitation via nad(p)h oxidase-dependent mitogen-activated protein kinase signaling. J Hypertens. 2010;28:806–816 [PubMed: 20027123]
62. Zarate S, Stevnsner T, Gredilla R. Role of estrogen and other sex hormones in brain aging. Neuroprotection and DNA repair. Front Aging Neurosci. 2017;9:430 [PubMed: 29311911]

Highlights

- TLR4 participates in a central feed-forward neuroinflammatory pro-hypertensive cycle
- TLR4 activation is required for BBB disruption in cardioregulatory nuclei
- TLR4 contributes to the development of autonomic dysfunction in hypertension
- TAK-242 is a promising therapeutic for the treatment of hypertension in males

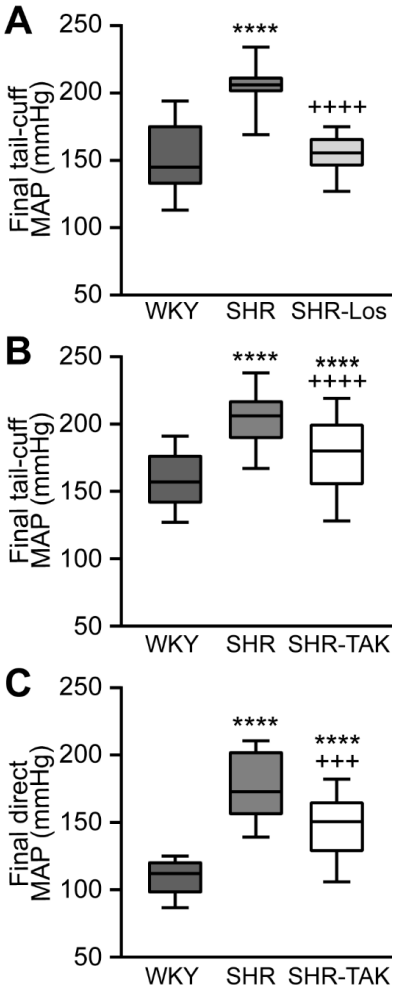

Figure 1 –. Progression of MAP elevation in SHRs is dependent upon AT1R and TLR4.

Final indirect tail-cuff mean arterial pressure (MAP; mmHg) measurements of Losartan cohort (n=6/group) (**A**) and TAK-242 cohort (n=11 WKY, 13 SHR, 17 SHR-TAK) (**B**) at conclusion of respective treatment periods; final direct MAP (mmHg) of TAK-242 sub-cohort (n=5 WKY, 6 SHR, 10 SHR-TAK; **C**). Data evaluated by one-way ANOVA with Tukey post-hoc analysis; data shown as mean±*SEM*; ****$p<0.0001$ vs. WKY; +++$p<0.001$ vs. SHR; ++++$p<0.0001$ vs. SHR.

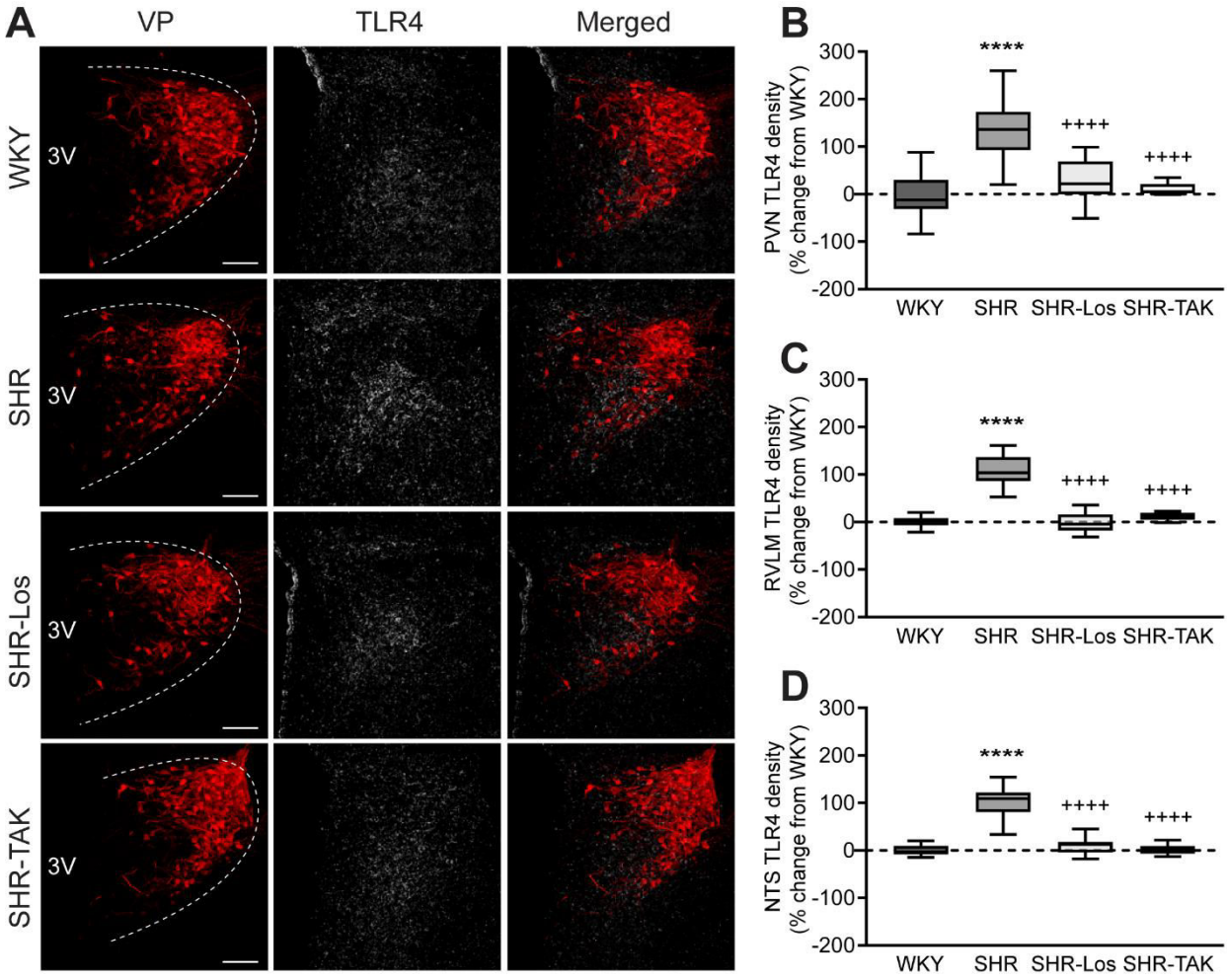

Figure 2 –. TLR4 protein expression within CNS cardioregulatory nuclei.

Example confocal maximum projection images of PVN vasopressin (VP; red) and TLR4 (white) from WKY, SHR, SHR-Los, and SHR-TAK (n=6/group) (**A**). Percent change in TLR4 staining (% area) compared to WKY in the PVN (**B**), RVLM (**C**), and NTS (**D**). Data evaluated by one-way ANOVA with Tukey post-hoc analysis; shown as mean±*SEM*; ****p<0.0001 vs. WKY; ++++p<0.0001 vs. SHR; scale bars: 100μm; 3V: third ventricle.

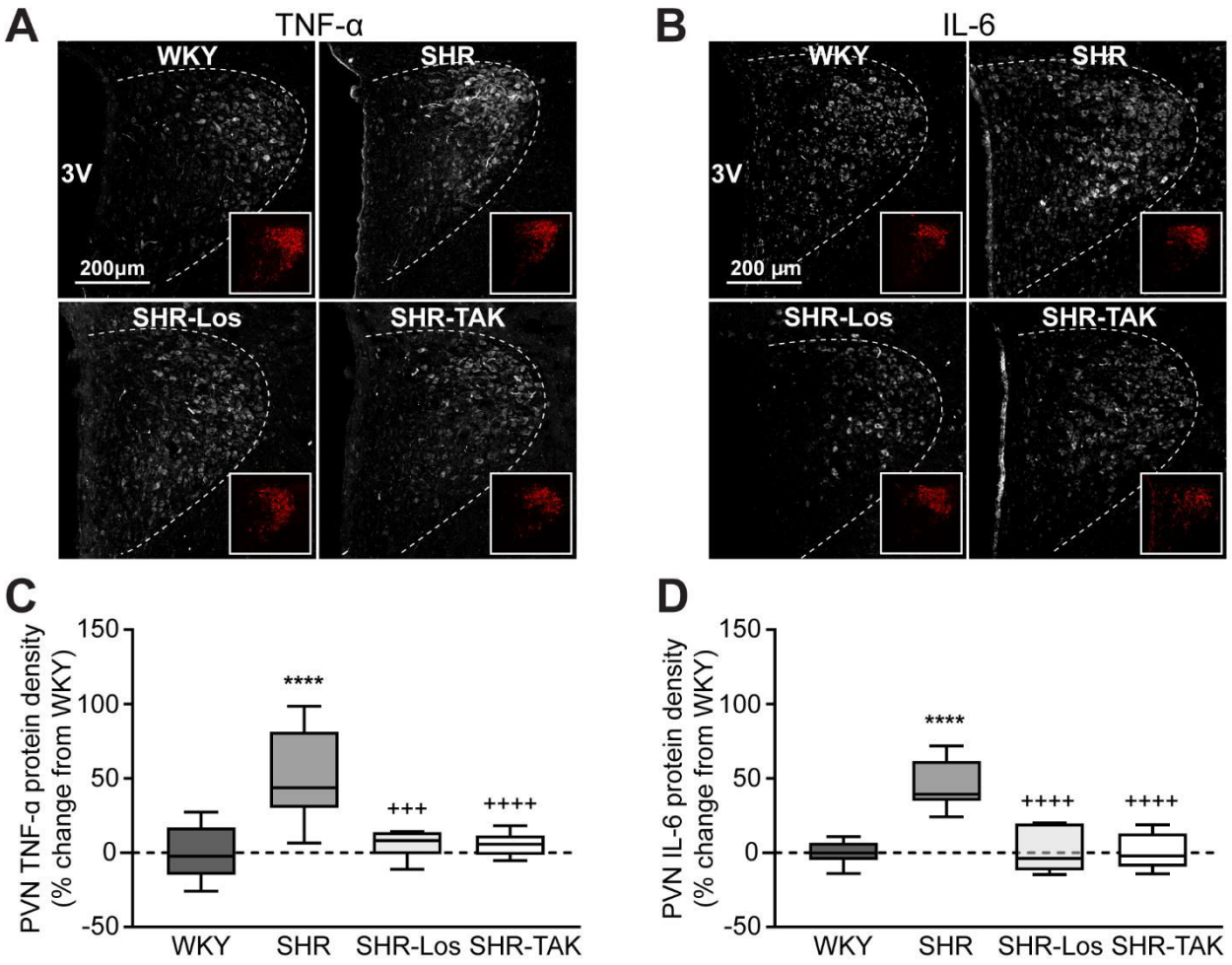

Figure 3 –. PVN pro-inflammatory cytokine density.

Example confocal maximum projection images of PVN TNF-α (**A**) and IL-6 (**B**) immunofluorescence (white) with respective anatomic marker, vasopressin (insets; red) in WKY, SHR, SHR-Los, and SHR-TAK (n=6/group). Box-plot diagrams of TNF-α (**C**) and IL-6 (**D**) protein density in the PVN, calculated as change in % area relative to WKY. Data evaluated by one-way ANOVA with Tukey post-hoc analysis; shown as mean±*SEM*; ****p<0.0001 vs. WKY; +++p<0.001 vs. SHR; ++++p<0.0001 vs. SHR; scale bars: 200μm; 3V: third ventricle.

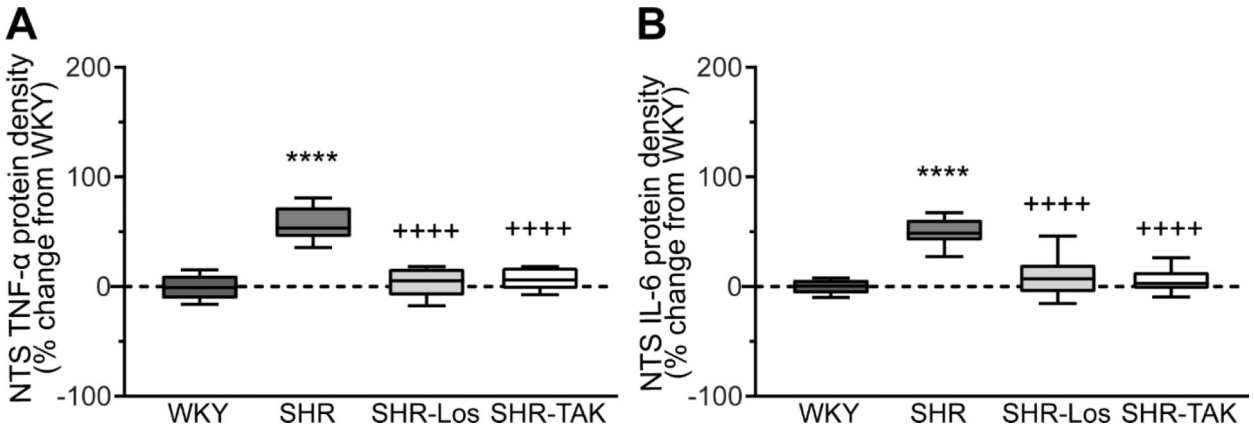

Figure 4 –. NTS pro-inflammatory cytokine density.

Box-plot diagrams of TNF-α (**A**) and IL-6 (**B**) protein density in the NTS of WKY, SHR, SHR-Los, and SHR-TAK (n=6/group), calculated as change in % area relative to WKY. Data evaluated by one-way ANOVA with Tukey post-hoc analysis; shown as mean±*SEM*; ***p*<0.01 vs. WKY; *****p*<0.0001 v.s WKY; ++++*p*<0.0001 vs. SHR.

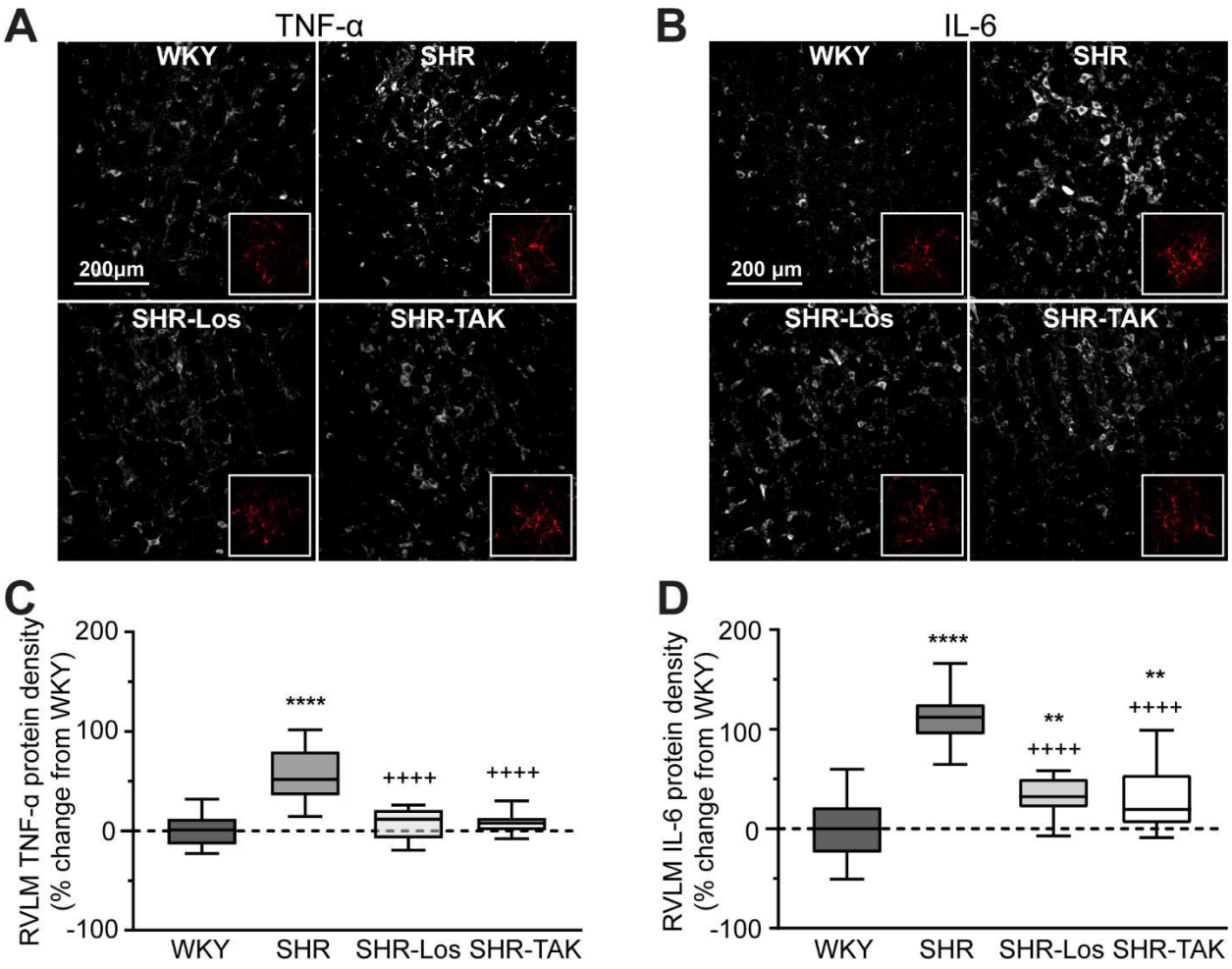

Figure 5 –. RVLM pro-inflammatory cytokine density.

Example confocal maximum projection images of RVLM TNF-α (**A**) and IL-6 (**B**) immunofluorescence (white) with respective anatomic marker, tyrosine hydroxylase (insets; red) in WKY, SHR, SHR-Los, and SHR-TAK (n=6/group). Box-plot diagrams of TNF-α (**C**) and IL-6 (**D**) protein density in the RVLM, calculated as change in % area relative to WKY. Data evaluated by one-way ANOVA with Tukey post-hoc analysis; shown as mean±*SEM*; ***p*<0.01 vs WKY; *****p*<0.0001 vs WKY; ++++*p*<0.0001 vs SHR; scale bars: 200μm.

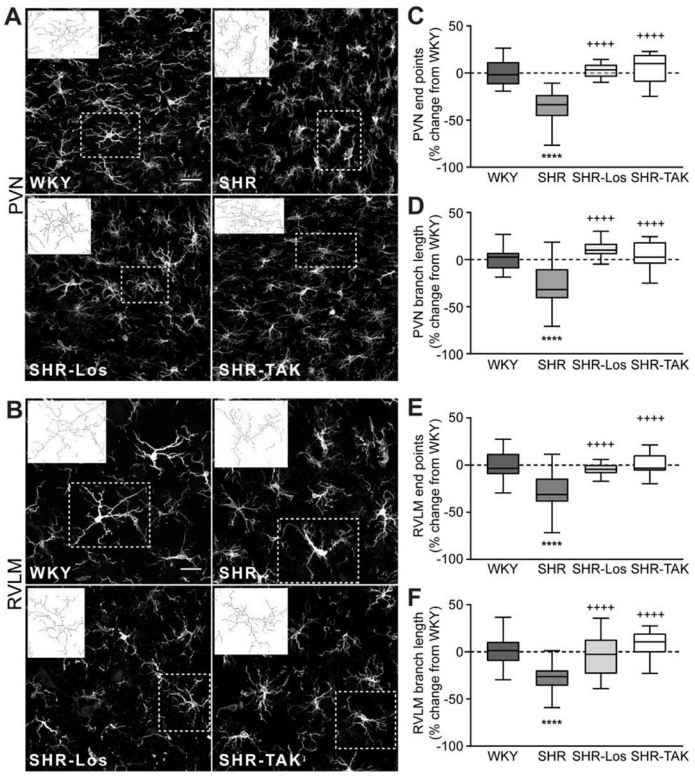

Figure 6 –. Skeletal analysis of microglial morphology in the PVN and RVLM.

Example confocal maximum projection images of IBA1 (microglial marker; white) in the PVN (**A**) and RVLM (**B**) of WKY, SHR, SHR-Los, and SHR-TAK (n=6/group). Maximum projection images were converted to binary and skeletonized, as illustrated by inset skeletons of outlined microglia. Percent change in PVN end points (**C**), PVN branch length (**D**), RVLM end points (**E**) and RVLM branch length (**F**) relative to WKY. Data evaluated by two-way ANOVA with Tukey post-hoc analysis; shown as mean±*SEM*; ****p<0.0001 vs. WKY; ++++p<0.0001 vs. SHR; scale bars: 50μm.

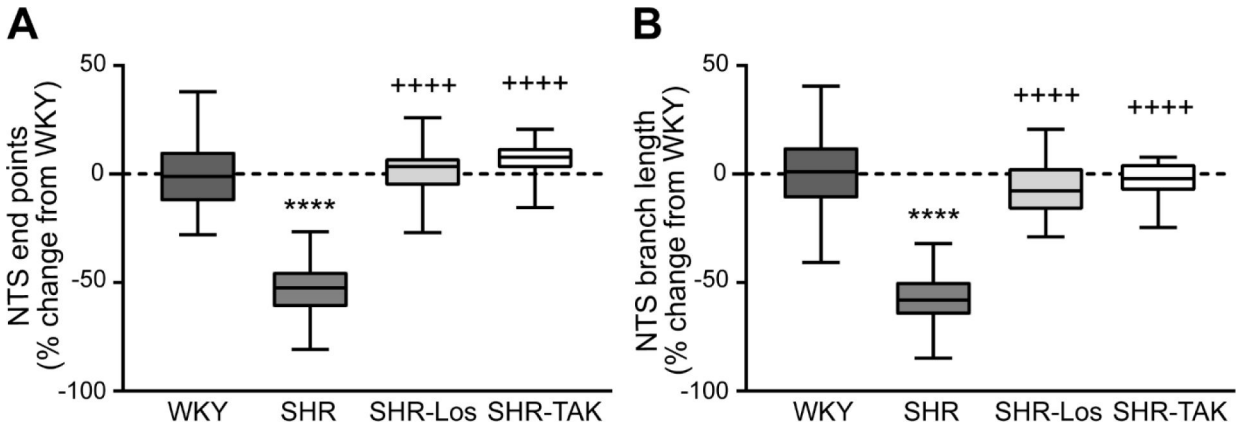

Figure 7 –. NTS microglial morphology.

Percent change in NTS end points (**A**) and branch length (**B**) relative to WKY in the NTS of WKY, SHR, SHR-Los, and SHR-TAK (n=6/group). Data evaluated by two-way ANOVA with Tukey post-hoc analysis; shown as mean±*SEM*; ****$p<0.0001$ vs. WKY; ++++$p<0.0001$ vs. SHR.

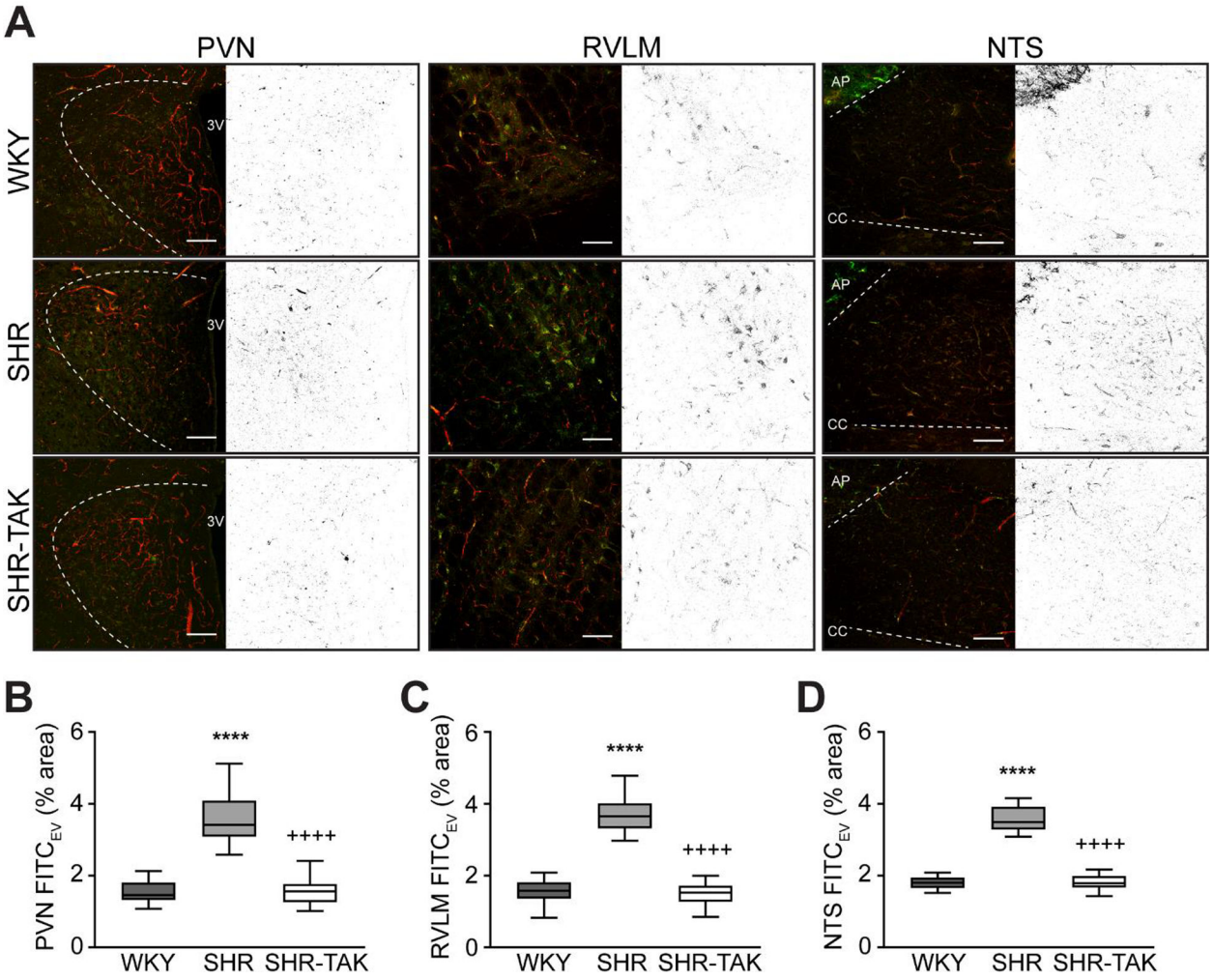

Figure 8 –. BBB permeability assessment in the PVN, RVLM, and NTS.

Example confocal maximum projection images showing FITC10 (green) and RHO70 (red) in the PVN, RVLM, and NTS (**A**) of WKY, SHR, and SHR-TAK (n=6/group), with corresponding images of extravasated FITC10 ($FITC10_{EV}$). Box-plot diagrams of $FITC10_{EV}$ (% area) in the PVN (**B**), RVLM (**C**), and NTS (**D**). Data evaluated by one-way ANOVA with Tukey post-hoc analysis; shown as mean±*SEM*; ****p<0.0001 vs. WKY; ++++p<0.0001 vs. SHR; scale bars: 100μm; 3V: third ventricle; AP: area postrema; CC: central canal.

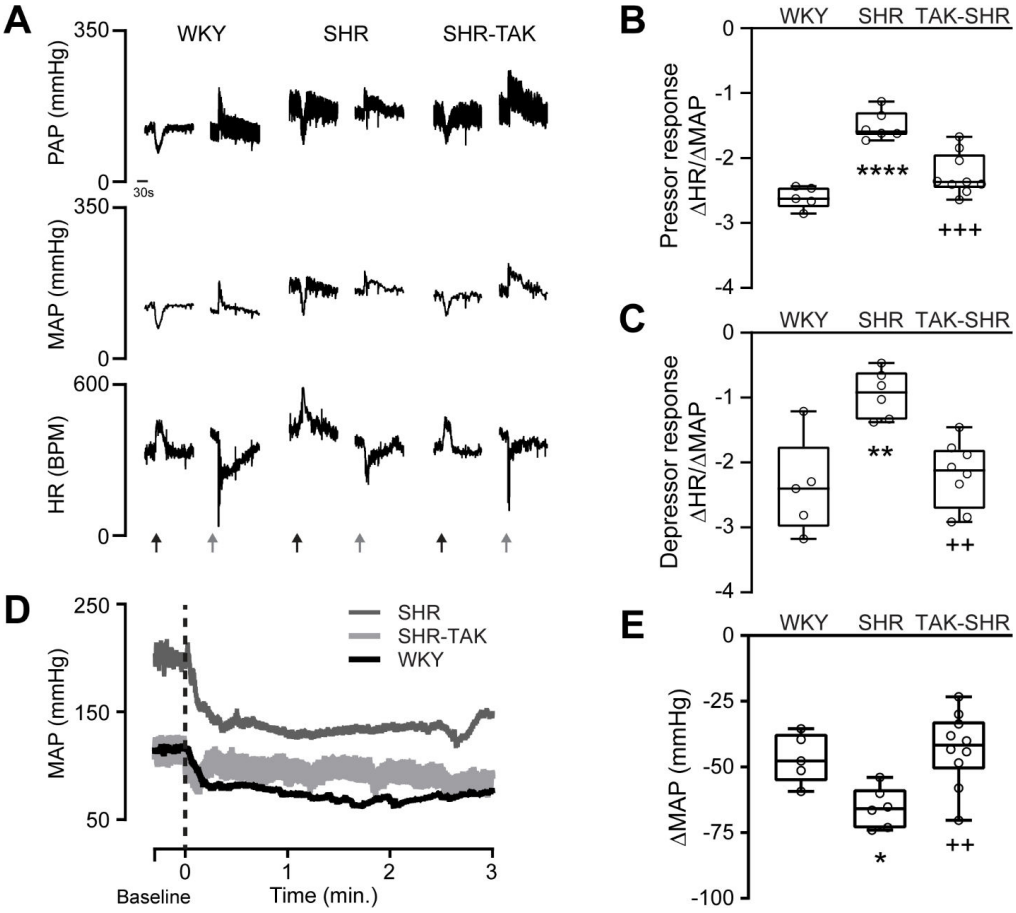

Figure 9 –. Baroreceptor reflex sensitivity assessment and indirect SNS activity.

Example tracings (**A**) of pulsatile arterial pressure (PAP; mmHg), mean arterial pressure (MAP; mmHg), and heart rate (HR; BPM), showing responses to injection of phenylephrine (gray arrows) and sodium nitroprusside (black arrows). Box-plot diagrams of pressor response to phenylephrine (**B**) and depressor response to sodium nitroprusside (**C**), calculated as ΔHR [BPM]/ΔMAP [mmHg]. Example tracings of MAP following ganglionic blockade with hexamethonium bromide injection (dashed line) (**C**), quantified as maximum ΔMAP from baseline (**D**) in WKY (n=5), SHR (n=6), and SHR-TAK (n=10). *p<0.05 vs. WKY; **p<0.01 vs. WKY; ****p<0.0001 vs. WKY; ++p<0.01 vs. SHR; ++++p<0.0001 vs. SHR.